JOURNAL OF Materials CHEMISTRY

A study on the effect of surface treatment of carbon nanotubes for liquid crystalline epoxide–carbon nanotube composites

Jyongsik Jang,*[a] Joonwon Bae[a] and Seong-Ho Yoon[b]

[a]*Hyperstructured Organic Materials Research Center, School of Chemical Engineering, College of Engineering, Seoul National University, Shinlimdong 56-1, Seoul, Korea. E-mail: jsjang@plaza.snu.ac.kr*
[b]*Institute of Advanced Materials Study, Kyushu University, Kasuga, Fukuoka 816-8580, Japan*

Received 12th December 2002, Accepted 16th January 2003
First published as an Advance Article on the web 10th February 2003

Chemical surface oxidation of carbon nanotubes was employed to modify the interfaces between liquid crystalline epoxide (LCE) molecules and carbon nanotubes (CNs). Polar functional groups are formed on the surfaces of the carbon nanotubes as a result of the treatment. The thermotropic behavior of the nematic liquid crystalline (LC) phase in liquid crystalline epoxide–carbon nanotube (LCE–CN) composites has been examined using polarized optical microscopy. The LC phase in the LCE–surface oxidized CN composite evolves at a lower temperature compared to that for LCE–CN, due to polar interactions. The mechanical properties of LCE–CN composites tend to increase with increasing CN content. The electrical conductivity of LCE–CN composites was found to increases dramatically compared to that of pristine LCE resin, up to 5 wt% CN loading, and then increase linearly with increasing CN content at high CN loadings. An investigation of the thermal properties of LCE–CNs in relation to the surface treatment of CNs was also undertaken. Surface oxidation of CNs was found to improve the mechanical durability and thermal stability of LCE–CN composites.

Introduction

Owing to their excellent electrical, mechanical, thermal, and magnetic properties, carbon nanotubes have been considered to be a new form of carbon material, and consist of concentric cylinders of graphite layers.[1] The diameters of CNs are 1000 times smaller than those of conventional carbon or reinforcement fibers. The high surface areas of CNs play a role in the effective reinforcement, unlike conventional carbon fillers. CNs have been studied for their potential applications in nanoscale devices and materials, field emission, and superconductors.[2–7] Recently, mass production of CNs has been achieved using arc discharge and laser ablation. The excellent electrical properties of CNs make them attractive candidates for new electronic devices.[8–10] Research[11–15] into the mechanical properties of CN composites has revealed that CNs can be potentially used as reinforcement fillers in polymer composite systems.

In the last few years, liquid crystalline epoxy resins have been synthesized and their cure kinetics and physical properties investigated.[16–19] A typical LCE is composed of an aromatic mesogenic group and a reactive oxirane ring, which takes part in the cross-linking reaction with an amine. The balance of properties between those of a liquid crystalline polymer and an epoxy resin means that these materials can be used as matrix resins for high performance polymer composites. For example, the epoxide functional group provides advantages such as versatility in the choice of curing agent and additive, excellent adhesion, and low shrinkage.

Ajayan *et al.*[24] initially fabricated epoxide–CN composites by mechanically mixing multi-walled carbon nanotubes in a polymer matrix. As hard conductive materials, LCE–CN composites show great potential for use as antistatic coatings or for electromagnetic shielding for electronic devices.[20–23] CNs offer an alternative for polymer matrix reinforcement[20–22] and enhance the electronic properties[8–10] of the resulting composite.

Although many studies have sought to improve the mechanical performance of polymer–CN composites, they provide only limited information concerning the surface modification of CNs. In particular, chemical surface oxidation of CNs may have important effects on the electrical, thermal, and mechanical properties of LCE–CN composites.

In this study, chemical oxidation of CNs was employed to modify the interface between CNs and LCE molecules in LCE–CN composites, to provide LCE–surface oxidized CN (oxCN) systems. The effect of oxidation of CNs on the thermotropic LC behavior of LCE–CN systems was also examined. The mechanical, electrical, and thermal properties of LCE–CN composites were investigated from the viewpoint of surface treatment of CNs.

Experimental

Materials

A liquid crystalline epoxy resin, the diglycidyl ether of 4,4′-dihydroxy-α-methyl stilbene (DGE-DHAMS) was employed as a matrix. The epoxide equivalent weight (EEW) of LCE is about 175. Sulfanilamide, the curing agent, was purchased from Aldrich and used as received. The structures of the LCE and the curing agent are shown in Fig. 1. The synthesis, physical, and chemical properties, and special applications of the LCE have been reported in the literature.[25–27]

Carbon nanotubes were employed as inorganic fillers in the LCE–CN composites. The carbon nanotubes were produced from the interaction of an iron catalyst with a CO–H_2 (4 : 1) mixture at 600 °C for 1 h. The general characteristics of the carbon nanotubes are presented in Table 1.

Synthesis of CNs

Multi-walled carbon nanotubes were prepared from a mixture of carbon monoxide and hydrogen gases (CO–H_2 4 : 1; v/v) on a

 DOI: 10.1039/b212190e

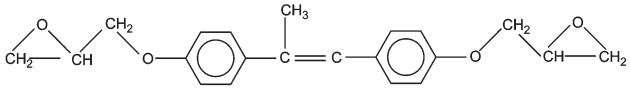

(a) diglycidyl ether of 4,4'-dihydroxy-α-methyl stilbene

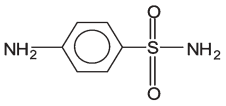

(b) sulfanilamide

Fig. 1 Chemical structures of (a) the liquid crystalline epoxy resin and (b) the curing agent.

Table 1 Preparation conditions and physical properties of carbon nanotubes

Preparation conditions		Physical properties	
Catalyst	Fe	Structure	Platelet
Reaction temperature/°C	600	Average diameter/nm	180
Reaction time/h	1	H/C (atomic ratio)	0.035
Gas composition ($CO–C_2H_2–H_2$; v/v)	4 : 0 : 1	d_{002} (XRD)/nm	0.3363
		Surface area/$m^2\ g^{-1}$	84

non-supported iron catalyst at a temperature of 600 °C using a conventional horizontal tube furnace. The iron catalyst powder used in this study was prepared *via* the precipitation of ferric carbonate by addition of ammonium bicarbonate, as described by Best and Russell.[6] The precipitate was dried overnight in an oven at 100 °C and then calcined in air at 400 °C for 5 h to convert the carbonate into the oxide. The calcined catalyst was reduced in a 10% H_2–He mixture for 20 h at 480 °C. The reduced catalyst was subsequently cooled to ambient temperature in a helium atmosphere before being passivated in a 5% air–He mixture for 1 h at room temperature. The passivated catalyst was then removed from the reactor and stored for later use. The quartz flow reactor used for the preparation of the CN was heated in a conventional horizontal tube furnace. The gas flow to the reactor was precisely monitored and regulated with MKS mass flow controllers. Powdered catalyst (30 mg) was placed in a quartz boat at the center of the reactor tube in the furnace. After reduction in a 10% H_2–He mixture for 2 h at the prescribed temperature, helium was flushed through the system for 0.5 h. The reactant gas, either a $CO–H_2$ or a $CO–CH_2CH_2–H_2$ mixture, was then allowed to flow over the catalyst. The total amount of carbon deposited after 1 h on stream was determined gravimetrically after cooling the system to ambient temperature. The prepared carbon was partially oxidized at 450 °C for 30 min under an air flow (100 ml min^{-1}), using the same type of horizontal furnace, to remove amorphous carbon on the surfaces of the CNs. Hydrogen (99.999%), carbon monoxide (99.9%), and He (99.99%) were obtained from MG industries and used without further purification. Reagent grade iron nitrate [$Fe(NO_3)_3{\cdot}9H_2O$], was obtained from Wako Chemical Co.

Characterization of CNs

The CNs were observed with high resolution transmission electron microscopes (HR-TEM; JEOL JEM 200CX and JEM-2001) with a bio-scan camera. The X-ray diffraction data were collected using a Rigaku Geigerflex instrument employing a Cu-Kα target, and the crystallographic parameters were calculated according to the Gakushin (JSPS) method.[7] Multipoint Brunauer–Emmett–Teller surface area measurements were made using a Coulter Omnisorb 100CX surface area analyzer. Prior to this measurement, the CNs were degassed at 150 °C for 8 h. A TEM image of CN is presented in Fig. 2.

Oxidation of CNs

The surfaces of CNs were oxidized in a preheated aqueous nitric acid solution (50–60%) at 100 °C for 30 min. Then, the CNs were refluxed with distilled water for 24 h and dried in a vacuum oven at 100 °C for 24 h.[28]

Preparation of sample mixture for curing

The mixtures were prepared by dissolving the LCE, the curing agent, and the filler in acetone. Then, the mixture was ultrasonicated for 1 h, and the solvent was evaporated. The molar ratio of epoxide to amide groups was fixed at 1. The samples are denoted as LCE for the epoxide–curing agent system, LCE–CN for the epoxide–carbon nanotube–curing agent system, and LCE–oxCN for epoxide–oxidized carbon nanotube–curing agent system. Ajayan and co-workers[2,23,24] reported that the efficient mixing of epoxy resin and CNs can be achieved by mechanical and sonication methods. The sample mixtures were cured at 150 °C for 4 h and post-cured at 175 °C for 1 h in a vacuum oven.

Instrumental analysis

The electrical conductivity of prepared samples was measured by the standard four-probe method under ambient conditions. The electrical conductivities were calculated using the formula,

$$\sigma = \frac{2\ln 2}{\pi g d(R_{12,34} + R_{23,41})}$$

where d is the thickness of sample in cm, $R_{12,34} = V_{34}/I_{12}$, $R_{23,41} = V_{41}/I_{23}$, and g is the correction factor.

The correction factor was determined from the value of $R_{12,34}/R_{23,41}$ using the correction factor curve. Fig. 3 shows the standard four-probe set-up and the correction factor curve used in order to measure the electrical conductivity of LCE–CN/oxCN specimens. FT-IR spectra were recorded on a Bomem MB100 spectrometer in absorption mode at a resolution of 4 cm^{-1} and are averages of 1200 scans. Thermogravimetric analysis (TGA) was performed using a Perkin Elmer TGA 7 instrument at a heating rate of 10 °C min^{-1} in N_2. Dynamic mechanical thermal analysis (DMTA) was conducted with a Rheometrics DMTA MK III analyzer.[17] The three-point bending method was employed at frequency of 1.0 Hz. The fabricated samples were heated from 10 to 250 °C at a heating rate of 5 °C min^{-1} in a chamber purged with nitrogen. LC phases were observed with a Leica MPS30

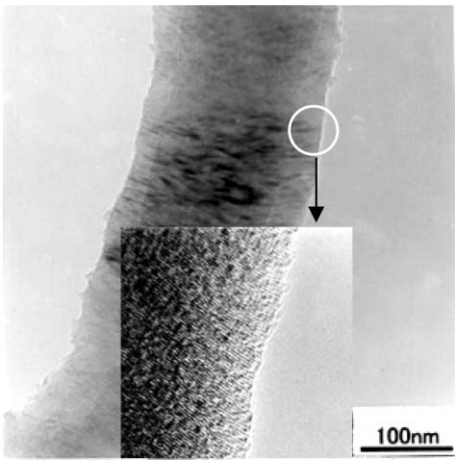

Fig. 2 TEM image of a carbon nanotube.

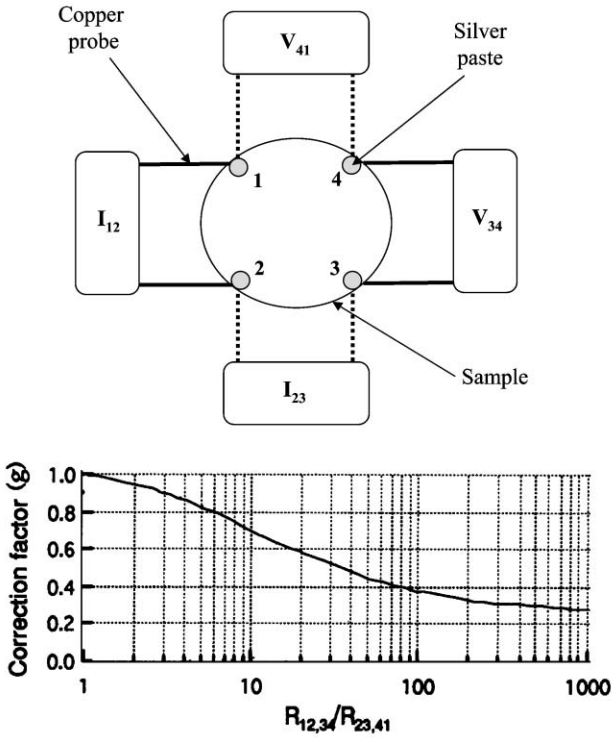

Fig. 3 Standard four-probe experimental set-up used to measure the electrical conductivity of epoxy resin–carbon nanotube composites and the plot of the correction factor, g, against $R_{12,34}/R_{23,41}$.

polarized optical microscope (POM) equipped with a Mettler Toledo FP82TH hot stage.

Results and discussion

Surface characteristics of CNs

The FT-IR spectra of pristine and surface-treated CNs are shown in Fig. 4. Because CNs are electrically conducting, the baselines in the spectra are slanted due to plasma reflection. The absence of hydroxyl and carbonyl groups in the pristine CNs is obvious from the IR spectrum [Fig. 4(a)]. On the other hand, charateristic bands due to generated polar functional groups are observed in the spectrum of oxidized CNs [Fig. 4(b)].[29] The vibrational band assignments are presented in Table 2.

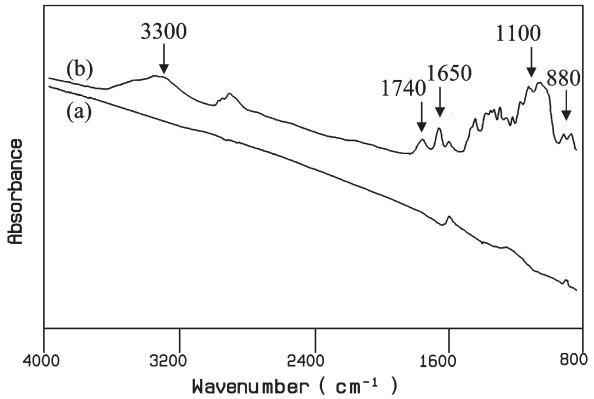

Fig. 4 FT-IR spectra of (a) pristine and (b) surface-treated carbon nanotubes. Peaks in the range 1000–1700 cm^{-1} in the latter correspond to the functional groups generated as a result of surface oxidation.

Table 2 Assignment of peaks in the IR spectrum of surface-treated carbon nanotubes

Vibrational band/cm^{-1}	Assignment
3300	OH str.[a] (medium)
2900–3000	CH str. (weak)
1720–1750	C=O str. (medium)
1640–1650	H-bonded C=O str. (weak)
1100–1200	C–C–O ring str., C–C–C asymmetric str.
850–900	C–C–C symmetric str.

[a]Stretching.

Morphological features and thermotropic LC behavior

The DSC curves of pristine LCE resin, LCE–CN, and LCE–oxCN are presented in Fig. 5. When the LCE resin is slowly cooled from the melting temperature of 130 °C, nematic LC domains form between 98 and 56 °C. These domains are not present at elevated temperatures between 100 and 130 °C; the isotropic state is merely observed.[25–27] Therefore, the exothermic peaks at higher temperature in Fig. 5 correspond to the isotropic-to-LC transition, and the peak at lower temperature in Fig. 5(c) is attributed to the LC-to-crystal transition. In the LCE–CN system, a nematic LC domain appears at 98 °C and is maintained to 56 °C, as reported by Earls and co-workers.[25–27] This phenomenon indicates that the LC domain in the LCE–CN system is not affected by the presence of CNs. However, the isotropic-to-LC transition temperature is shifted to a lower temperature in the LCE–oxCN system. The exothermic peak in Fig. 5(c) is weak compared with that in Fig. 5(b).

The different behavior of the LC domain in LCE–oxCN is attributed to the effect of surface oxidation of the CNs. Oxidation of the carbon materials generates polar groups, such as O–H, C=O, and N–H, on the surface.[28,29] Because the epoxide groups in LCE molecules are electrophiles (E^+) and the generated polar groups are nucleophiles (Nu^-), they can form E^+–Nu^- complexes.[29]

As shown in Fig. 5(b), the LC domain evolves at 98 °C in LCE–CN. This means that the molecular alignment of LCE molecules required for the formation of the LC domain appears at this temperature; the mesogenic groups of the LCE molecules start to align spontaneously. In contrast, polar interactions between the epoxides and the nanotube surface functional groups occurs in the LCE–oxCN. The molecular motions of the epoxides for evolution of the LC phase are partially restricted by these polar interactions. In the case of the LCE–oxCN composite, the LC domain cannot form at

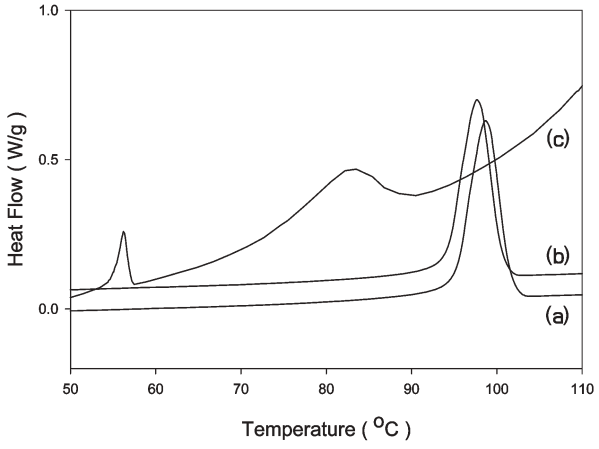

Fig. 5 DSC curves for (a) LCE, (b) LCE–CN (5 wt%), and (c) LCE–oxCN (5 wt%) systems. In the DSC experiments, samples were heated from 20 to 130 °C at a heating rate of 10 °C min^{-1}, and cooled to 50 °C at a rate of 5 °C min^{-1} in nitrogen. The DSC curves were obtained during the cooling scan.

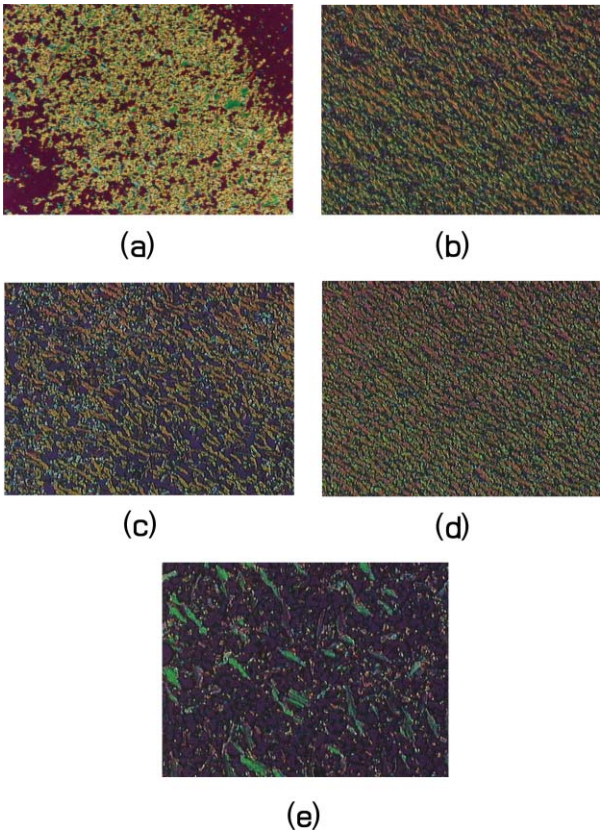

Fig. 6 POM images of LCE–CN systems: (a) LCE (99 °C); (b) LCE–CN (5wt%, 98 °C); (c) LCE–oxCN (5 wt%, 83 °C); (d) LCE–oxCN (20 wt%, 81 °C); (e) onset of the LC domain in LCE–oxCN (5 wt%, 83 °C). The LC domain was observed using the same heating–cooling cycle as for the DSC experiments.

98 °C. At lower temperature, the intermolecular distance between LCE molecules becomes less and intermolecular steric hindrance occurs. In order to reduce this, forced packing of the LCEs and LCE^{+}–CN^{-} complexes is promoted. Therefore, the LC phase in LCE–oxCN evolves at a lower temperature compared to LCE–CN.

POM images of LCE–CN systems are presented in Fig. 6. Judging from the images, the nematic LC phase is formed with different CN and oxCN contents.[25,26] It has been reported that the orientation of LCE molecules on the surface of carbon fibers (CFs) is promoted when the carbon fiber is introduced as a filler.[30–33] In this study, CNs were employed instead of CFs, but the orientation of LCE molecules on the CN surfaces can be expected according to the same mechanism.[30–33] Specific interactions between the epoxides and the polar groups on the surfaces of the CNs promote the formation of LCE layers on the surfaces of the CNs. Therefore, orientation of the LCE molecules along the CNs is facilitated. Structural features like a high aspect ratio make CNs better fillers than carbon blacks.

Mechanical properties of LCE–CN composites

The mechanical properties of cured LCE–CN composites were investigated using DMTA. Fig. 7 shows the storage moduli of LCE–CN composites as a function of CN content. The LCE–CN composites were cured at 150 °C for 4 h and maintained at 175 °C for 1 h for post curing. In general, the modulus of thermoset resins is mainly affected by the chemical structure, the degree of curing, and the curing temperature.[16–19] The moduli of LCE–CN composites tends to increase with increasing CN content.[11] Since the LCE–CN composites were fabricated at the same curing temperature, the changes in the storage modulus are mainly due to the increasing CN content. It is noteworthy that the modulus of the LCE–CN

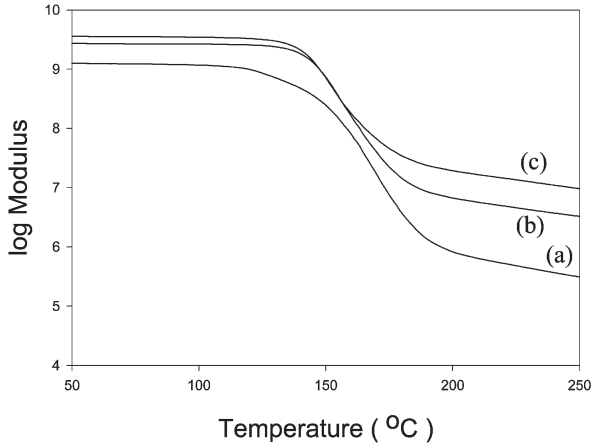

Fig. 7 DMTA thermograms of LCE–CN systems with different CN contents obtained at frequency of 1.0 Hz: (a) 1 wt% CN; (b) 10 wt% CN; (c) 20 wt% CN. The fabricated samples were heated from 10 to 250 °C at a heating rate of 5 °C min^{-1}.

composites does not depend on the degree of curing to any significant degree.[29]

Fig. 8 shows the moduli of LCE–CN and LCE–oxCN composites. The samples were again cured at 150 °C for 4 h and post cured at 175 °C for 2 h. The post curing time was increased for complete curing of the composites. Surface treatment of carbon fibers, which improved the interfacial interaction between the epoxide matrix and the carbon fibers, has been found to affect the dynamic mechanical properties of LCE–CF composites.[16–19] The nitric acid treatment generated polar functional groups on the CN surface. The modulus of LCE–oxCN increases slightly below the transition region, and increases above the transition region compared with LCE–CN. This phenomenon can be explained by the fact that surface treatment of CNs promotes the polar interaction between the CN surface and the epoxy resin. The formation of polar interactions in the interfacial region alters the relaxation behavior and broadens the transition region. This means that improved interfacial adhesion restrains the molecular motion of LCE molecules at the interface. Generally, heat-resistant composites, such as benzoxazine–CF, polyimide–CF, and epoxide–CF show a large drop in modulus in the transition region.[17] In the case of the LCE–oxCN composite, the decrease in modulus drop near transition region can be assumed to be due to the inhibition of the molecular motion of the LCE molecules.

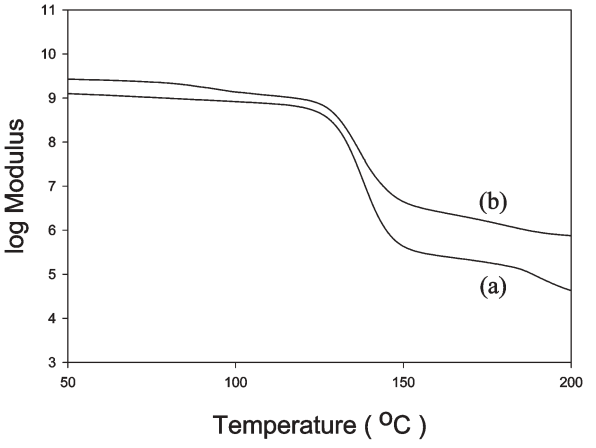

Fig. 8 DMTA thermograms of (a) LCE–CN and (b) LCE–oxCN composites containing 1 wt% of CNs or oxCNs, respectively. The sample mixtures were cured at 150 °C for 4 h and post-cured at 175 °C for 2 h to increase the degree of curing.

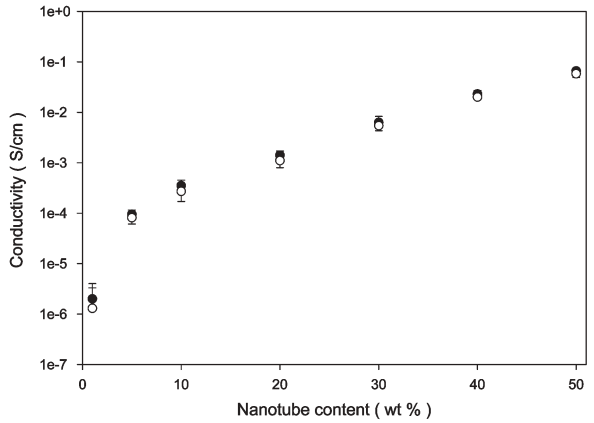

Fig. 9 Electrical conductivity of LCE–CN (●) and LCE–oxCN (○) composites as a function of CN content.

Electrical conductivity of LCE–CN composites

Windle *et al.*[34] have investigated the electrical properties of epoxide–carbon nanotube composites with low carbon nanotube loadings, and reported the percolation threshold behavior of the electrical conductivity. In this study, the electrical conductivity of LCE–CN composites was examined over a wide range of CN loadings (Fig. 9). In the case of low CN content (below 10 wt%), the electrical conductivity of LCE–CN composites increases dramatically compared to cured LCE resin. This indicates that the LCE–CN composites show a kind of percolation threshold behavior. Owing to their nanoscale architecture, the CNs are minutely dispersed in the polymer matrix, although regional aggregation of CNs might occur in a limited space. It is noteworthy that the electrical conductivity of LCE–CN composites increased linearly with increasing CN content at high CN loading. The surface oxidation of CNs did not increase the electrical conductivity of LCE–oxCN composites compared to the LCE–CN composites. This means that the electrical conductivity of LCE–CN and LCE–oxCN materials is dependent on the intrinsic electrical conductivity of the CNs.

Thermal stability of LCE–CN composites

Fig. 10 shows the TGA thermograms of LCE–CN composites as a function of CN content. The initial degradation temperatures of the composites are slightly higher than that of pristine LCE–amine, and the thermal degradation temperature is independent of CN content. The residual mass increased with increasing CN content.

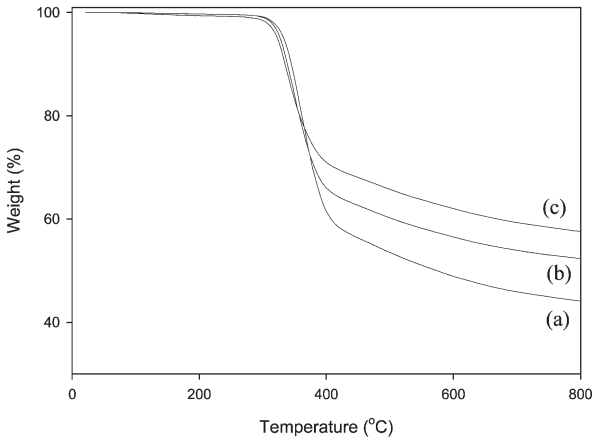

Fig. 10 TGA thermograms of LCE–CN systems with different CN contents obtained at a heating rate of 10 °C min^{-1} in N_2: (a) 10 wt% CN; (b) 30 wt% CN; (c) 50 wt% CN.

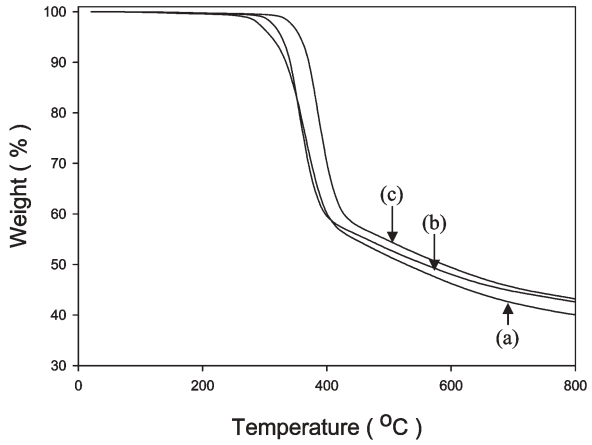

Fig. 11 TGA thermograms of LCE–CN systems obtained at a heating rate of 10 °C min^{-1} in N_2: (a) LCE; (b) LCE–CN (1 wt%); (c) LCE–oxCN (1 wt%).

Since the epoxide/amine molar ratio was kept constant in all the LCE–CN composites, the degree of LCE curing should be almost constant.[29] While the LCE curing rate in the LCE–CN system decreases as the CN content increases, the final degree of curing is almost the same under experimental conditions due to the complete curing of LCE.[29] This means that the thermal stability of the cross-linked epoxide network is not affected by the CN content. Although the interfacial interaction between the CNs and the epoxide network increases with increasing CN content, the thermal resistivity of LCE–CN composite does not improve significantly.

TGA experiments were performed in order to examine the effect of surface treatment of CNs on the thermal resistance of LCE–CN composites. Fig. 11 shows the TGA thermograms of pristine LCE, LCE–CN, and LCE–oxCN. The thermal degradation temperature of LCE–oxCN is higher than that of LCE–CN. As reported previously,[28,29] functional groups such as COOH, C=O, and OH are generated on the CNs as a result of surface treatment. These functional groups have some nucleophilicity, which induces polar interactions with the electrophilic epoxide groups.[29] Nucleophile–electrophile complexes can then be formed between functional groups and epoxides due to these polar interactions. The dispersion of CNs is promoted[29] and the cleavage of the epoxide ring facilitated. In the polymer–carbon nanotube system, homogeneous dispersion of carbon nanotubes in the polymer matrix is a critical factor for improving the performance of materials. Surface treatment of CNs is a facile way to disperse CNs more effectively in an LCE matrix. In addition, the thermal stability of LCE–oxCN composites is improved through the surface treatment of the CNs because the molecular motions of the LCE molecules are restricted by attractive polar interactions.

Conclusions

The effect of surface treatment of carbon nanotubes in their composites with liquid crystalline epoxy resins has been examined. Chemical surface oxidation of CNs improves interfacial adhesion between them and LCE molecules. In the case of LCE–oxCN composites, the nematic LC phase evolved at a lower temperature compared to that of the LCE–CN composite due to polar interactions between the surface-modified nanotubes and the epoxide matrix. The moduli of LCE–CN composites tends to increase with increasing CN content, and their electrical conductivity increases dramatically compared to that of cured LCE resin up to 5 wt% CN loading. In addition, the thermal stability of LCE–oxCN composites is

also improved due to the aforementioned attractive polar interaction.

Acknowledgement

The work was financially supported by the Brain Korea 21 program. (The Korean Ministry of Education and Korea Science and Engineering Foundation through the Hyperstructured Organic Materials Research Center.)

References

1 S. Iijima, *Nature*, 1991, **354**, 56.
2 T. W. Ebbesen and P. M. Ajayan, *Nature*, 1992, **358**, 220.
3 C. Downs, J. Nugent, P. M. Ajayan, D. J. Duquett and K. S. V. Santhanam, *Adv. Mater.*, 1999, **11**, 1028.
4 H. Ago, K. Petritsch, M. S. P. Shaffer, A. H. Windle and R. H. Friend, *Adv. Mater.*, 1999, **11**, 1281.
5 Z. Jin, X. Sun, G. Xu, S. H. Goh and W. Ji, *Chem. Phys. Lett.*, 2000, **318**, 505.
6 R. J. Best and W. W. Russell, *J. Am. Chem. Soc.*, 1954, **76**, 838.
7 *Tanso*, 1963, **36**, 25.
8 S. A. Curran, P. M. Ajayan, W. J. Blau, D. L. Carroll, J. N. Coleman, A. B. Dalton, P. Davey, A. Drury, B. Mccarthy, S. Maier and A. Strevens, *Adv. Mater.*, 1998, **10**, 1091.
9 H. S. Woo, R. Czerw, S. Webster, D. L. Carroll, J. Ballato, A. E. Strevens, D. O'Brien and W. Blau, *Appl. Phys. Lett.*, 2000, **77**, 1393.
10 Y. H. Lee, D. H. Kim, H. Kim and B. K. Ju, *J. Appl. Phys.*, 2000, **88**, 4181.
11 X. Gong, J. Liu, S. Baskaran, R. D. Voise and J. S. Young, *Chem. Mater.*, 2000, **12**, 1049.
12 R. Andrews, D. Jacques, A. M. Rao, T. Rantell and F. Derbyshire, *Appl. Phys. Lett.*, 1999, **75**, 1329.
13 H. Dai, J. Kong, C. Zhou, N. Franklin, T. Tombler, A. Cassell, S. Fan and M. Chaplin, *J. Phys. Chem. B*, 1999, **103**, 11246.
14 M. A. Hamon, J. Chen, H. Hu, Y. Chen, M. E. Itkis, A. M. Rao, P. C. Eklund and R. C. Haddon, *Adv. Mater.*, 1999, **11**, 834.
15 L. Dai, *Polym. Adv. Technol.*, 1999, **10**, 357.
16 J. Jang, S. C. Kim and J. Y. Lee, *Macromol. Rapid Commun.*, 2000, **21**, 960.
17 J. Y. Lee and J. Jang, *J. Polym. Sci., Part A: Polym. Chem.*, 1999, **37**, 419.
18 C. Ortiz, R. Kim, E. Rodighiero, C. K. Ober and E. J. Kramer, *Macromolecules*, 1998, **31**, 4074.
19 B. Szczepaniak, K. C. Frisch, P. Penczek, J. Rejdych and A. Winiarska, *J. Polym. Sci., Part B: Polym. Phys.*, 1997, **35**, 2739.
20 R. Haggenmueller, H. H. Gommans, A. G. Rinzler, K. I. Winey and J. E. Fischer, *Chem. Phys. Lett.*, 2000, **330**, 219.
21 S. P. Milo and A. H. Windle, *Adv. Mater.*, 1999, **11**, 937.
22 M. Yin, J. A. Koutsky, T. L. Barr, N. M. Rodriguez, R. T. K. Baker and L. Klebanov, *Chem. Mater.*, 1993, **5**, 1024.
23 P. M. Ajayan, *Chem. Rev.*, 1999, **99**, 1787.
24 P. M. Ajayan, O. Stephen, C. Colliex and D. Trauth, *Science*, 1994, **265**, 1212.
25 H.-J. Sue, J. D. Earls and R. E. Hefner, *J. Mater. Sci.*, 1997, **32**, 4031.
26 H.-J. Sue, J. D. Earls and R. E. Hefner, *J. Mater. Sci.*, 1997, **32**, 4039.
27 J. D. Earls, R. E. Hefner Jr. and P. M. Puckett, *US Pat.*, 5 463 091, 1995.
28 M. S. P. Shaffer, X. Fan and A. H. Windle, *Carbon*, 1998, **36**, 1603.
29 J. Bae, J. Jang and S.-H. Yoon, *Macromol. Chem. Phys.*, 2002, **203**, 2196.
30 J. J. Mallon and P. M. Adams, *Mol. Cryst. Liq. Cryst.*, 1991, **208**, 65.
31 J. J. Mallon and P. M. Adams, *Mol. Cryst. Liq. Cryst.*, 1992, **213**, 173.
32 C. Carfagna, D. Acierno, V. D. Palma, E. Amendola and M. Giamberini, *Macromol. Rapid Commun.*, 2000, **201**, 2631.
33 C. Carfagna, D. Acierno, V. D. Palma, E. Amendola and M. Giamberini, *Macromol. Rapid Commun.*, 2000, **201**, 2639.
34 J. Sandler, M. S. P. Shaffer, T. Prasse, W. Bauhofer, K. Schulte and A. H. Windle, *Polymer*, 1999, **40**, 5967.